AMERICAN SOCIETY FOR MICROBIOLOGY | mBio®

RESEARCH ARTICLE
Host-Microbe Biology

Formate Promotes *Shigella* Intercellular Spread and Virulence Gene Expression

Benjamin J. Koestler,[a] Carolyn R. Fisher,[a] Shelley M. Payne[a]

[a]Department of Molecular Biosciences and Institute for Cellular and Molecular Biology, The University of Texas at Austin, Austin, Texas, USA

ABSTRACT The intracellular human pathogen *Shigella flexneri* invades the colon epithelium, replicates to high cell density within the host cell, and then spreads to adjacent epithelial cells. When *S. flexneri* gains access to the host cytosol, the bacteria metabolize host cytosolic carbon using glycolysis and mixed acid fermentation, producing formate as a by-product. We show that *S. flexneri* infection results in the accumulation of formate within the host cell. Loss of pyruvate formate lyase (PFL; Δ*pflB*), which converts pyruvate to acetyl coenzyme A (CoA) and formate, eliminates *S. flexneri* formate production and reduces the ability of *S. flexneri* to form plaques in epithelial cell monolayers. This defect in PFL does not decrease the intracellular growth rate of *S. flexneri*; rather, it affects cell-to-cell spread. The *S. flexneri* Δ*pflB* mutant plaque defect is complemented by supplying exogenous formate; conversely, deletion of the *S. flexneri* formate dehydrogenase gene *fdnG* increases host cell formate accumulation and *S. flexneri* plaque size. Furthermore, exogenous formate increases plaque size of the wild-type (WT) *S. flexneri* strain and promotes *S. flexneri* cell-to-cell spread. We also demonstrate that formate increases the expression of *S. flexneri* virulence genes *icsA* and *ipaJ*. Intracellular *S. flexneri icsA* and *ipaJ* expression is dependent on the presence of formate, and *ipaJ* expression correlates with *S. flexneri* intracellular density during infection. Finally, consistent with elevated *ipaJ*, we show that formate alters *S. flexneri*-infected host interferon- and tumor necrosis factor (TNF)-stimulated gene expression. We propose that *Shigella*-derived formate is an intracellular signal that modulates virulence in response to bacterial metabolism.

IMPORTANCE *Shigella* is an intracellular pathogen that invades the human host cell cytosol and exploits intracellular nutrients for growth, enabling the bacterium to create its own metabolic niche. For *Shigella* to effectively invade and replicate within the host cytoplasm, it must sense and adapt to changing environmental conditions; however, the mechanisms and signals sensed by *S. flexneri* are largely unknown. We have found that the secreted *Shigella* metabolism by-product formate regulates *Shigella* intracellular virulence gene expression and its ability to spread among epithelial cells. We propose that *Shigella* senses formate accumulation in the host cytosol as a way to determine intracellular *Shigella* density and regulate secreted virulence factors accordingly, enabling spatiotemporal regulation of effectors important for dampening the host immune response.

KEYWORDS *Shigella*, formate, metabolism, virulence regulation

Shigella flexneri is an enteropathogenic subspecies of *Escherichia coli* that causes shigellosis, an acute mucosal inflammation resulting in severe bloody dysentery. After ingestion, *Shigella* traverses the digestive tract to the colon and crosses the colonic epithelium by exploiting M cells (1); the bacteria then invade the basolateral face of the epithelium using a contact-dependent type 3 secretion system (T3SS) encoded on a virulence plasmid, causing epithelial cells to engulf the bacteria. After

Received 16 August 2018 **Accepted** 20 August 2018 **Published** 25 September 2018

Citation Koestler BJ, Fisher CR, Payne SM. 2018. Formate promotes *Shigella* intercellular spread and virulence gene expression. mBio 9:e01777-18. https://doi.org/10.1128/mBio.01777-18.

Editor Bonnie Bassler, Princeton University

Copyright © 2018 Koestler et al. This is an open-access article distributed under the terms of the Creative Commons Attribution 4.0 International license.

Address correspondence to Benjamin J. Koestler, bkoestler@austin.utexas.edu.

This article is a direct contribution from a Fellow of the American Academy of Microbiology. Solicited external reviewers: Marcia Goldberg, Harvard Medical School; Barry Bochner, Biolog.

Shigella enters the cell and escapes the host engulfment vacuole, it multiplies within the host cell cytoplasm and subsequently spreads to adjacent cells using the protein IcsA (also known as VirG), which catalyzes host actin synthesis, propelling the bacterium into neighboring cells (2, 3).

Expression of *S. flexneri* virulence genes inside the host epithelial cell is dynamic. Although initially required for invasion, T3SS genes are repressed upon entry into the host epithelial cell (4–6). The T3SS genes and additional cell-to-cell spread genes are later reactivated through an unidentified mechanism immediately prior to spread (6). *S. flexneri* expresses a suite of T3SS effectors to dampen the host response to cytosolic infection. The effectors IpgD, OspI, OspG, OspF, and IpaH work in concert to modulate inflammation (7, 8). Host intracellular trafficking, which alters both epithelial cell homeostasis and defense against cytosolic bacteria, is another target of *S. flexneri*-secreted effectors. The secreted effector IpaB redirects host cholesterol away from the Golgi apparatus, resulting in Golgi fragmentation (9). Likewise, the secreted effectors VirA and IpaJ alter Golgi apparatus-mediated cell trafficking (10, 11). IpaJ is a cysteine protease that alters N-myristoylation (11), ultimately inhibiting the trafficking of STING, a known host cytosolic sensor of *S. flexneri* infection (12, 13). This results in blocking the STING-mediated activation of the type I interferon response, including cytokines such as CXCL10 (11, 12).

S. flexneri differentially regulates over a quarter of its genes in the intracellular environment compared to *S. flexneri* grown *in vitro*, including many genes involved in central carbon metabolism (5, 14). *S. flexneri* tricarboxylic acid (TCA) cycle enzymes are repressed in the intracellular environment, whereas enzymes involved in glycolysis and mixed acid fermentation pathways are increased and necessary for virulence (15–17). Specifically, *pflB*, the gene encoding pyruvate formate lyase (PFL), and PFL-associated genes are upregulated in the host cell (5, 15). PFL converts pyruvate to acetyl coenzyme A (CoA), producing formate as a by-product. An *S. flexneri* Δ*pflB* mutant is defective in plaque formation; however, deletion of *pflB* does not impact *S. flexneri* growth rate within the host cell (15, 16).

The scope of this study was to determine the role of *S. flexneri* formate metabolism in virulence during the host-cytosolic phase of infection. We propose a model where *Shigella*-derived formate accumulates in the host cell cytoplasm and promotes the expression of IcsA and IpaJ, linking *S. flexneri* metabolism and intracellular cell density to intercellular spread and host-pathogen response.

RESULTS

Formate promotes *S. flexneri* plaque formation in Henle-407 monolayers. One measure of *S. flexneri* virulence is the ability of *S. flexneri* to form plaques in cultured epithelial cell monolayers, which is contingent on both the ability of *S. flexneri* to replicate intracellularly and its ability to spread to adjacent host cells (18). Previous studies have shown that failure to form plaques, or formation of smaller-than-wild-type (WT) plaques, correlates with decreased virulence in animal models (18–20). An *S. flexneri* Δ*pflB* mutant forms smaller plaques in Henle-407 monolayers than does WT *S. flexneri* (15). Consistent with a previous study (16), the *S. flexneri* Δ*pflB* mutant showed no intracellular growth defect (see Fig. S1 in the supplemental material). Although not statistically different, the doubling time of the mutant was slightly shorter; as such, any effect of this small difference in growth over the time of plaque formation would be expected to lead to larger, rather than smaller, plaques. This suggested that formate, a product of PFL, secreted by *S. flexneri* promoted plaque formation independently of bacterial growth. If the plaque defect in the *pflB* mutant was due solely to the loss of formate, providing exogenous formate should rescue the Δ*pflB* plaque defect. At biological pH, formate cannot passively diffuse across bacterial or eukaryotic cell membranes (21). However, a previous study showed that exogenously supplemented formate could be taken up by cultured cells (22), and we confirmed that that Henle-407 cells take up radiolabeled formate when supplemented in tissue culture medium (Fig. S2). We supplemented tissue culture medium of cells infected with the *S. flexneri*

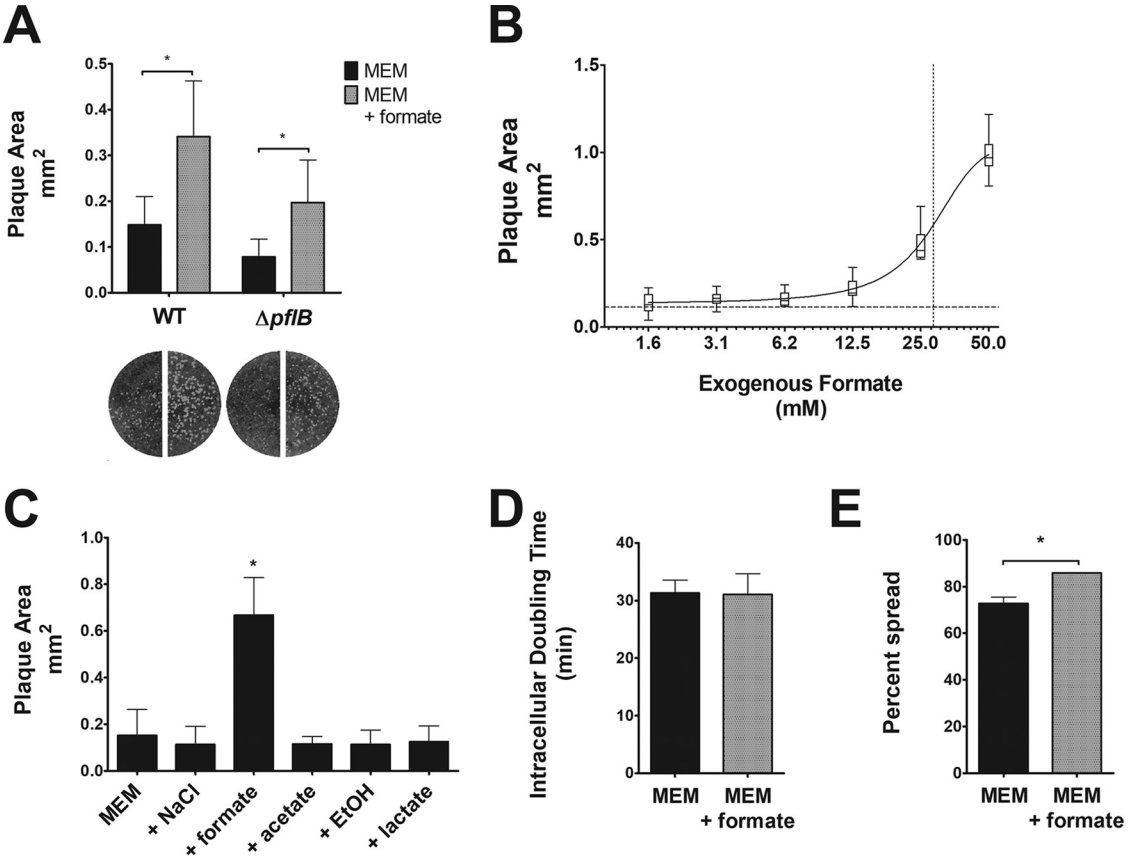

FIG 1 Formate-induced increase in *S. flexneri* cell-to-cell spread. (A) Wright-Giemsa stain of Henle-407 monolayers infected with *S. flexneri* and *S. flexneri* Δ*pflB* mutant with or without 20 mM formate. Plaque sizes were measured; an asterisk indicates statistical significance. (B) Plaque size of *S. flexneri* was measured when various concentrations of formate were added as supplements. The dotted line on the *y* axis indicates the plaque area when no formate was added as a supplement (0.1 mm^2), while the dotted line on the *x* axis indicates the 50% effective concentration (28.4 mM). (C) Plaque size of *S. flexneri* was measured with 20 mM NaCl, formate, acetate, ethanol, or lactate; an asterisk indicates a statistically significant difference from MEM. Only formate was found to increase *S. flexneri* plaque size. (D) *S. flexneri* intracellular doubling time was measured in Henle-407 cells with or without 20 mM formate. (E) *S. flexneri* cell-to-cell spread was measured at 3 hpi with or without 20 mM formate; an asterisk indicates statistical significance.

PFL mutant (Δ*pflB*) with 20 mM formate after *S. flexneri* invasion and measured plaque formation. In the absence of exogenous formate, the average Δ*pflB* plaque size was approximately half the size of the WT strain (Fig. 1A), consistent with previous observations (14). However, with the addition of exogenous formate, the plaque size of the Δ*pflB* mutant was restored to WT size (Fig. 1A), suggesting that *S. flexneri*-derived formate promotes *S. flexneri* plaque formation. Additionally, the plaque size of the WT strain increased 2.3-fold in the presence of exogenous formate (Fig. 1A). The formate concentration used in these experiments is in the midrange of the dose-response curve (Fig. 1B) and is within the range found in the mammalian gastrointestinal tract (23–26).

To determine if other fermentation by-products promote *S. flexneri* plaque formation, the medium of *S. flexneri*-infected Henle-407 cells was supplemented with 20 mM formate, acetate, ethanol, or lactate. With the exception of ethanol, these compounds were provided as supplements as sodium salts; thus, we included a control supplemented with 20 mM NaCl. Exclusively in the presence of formate, we observed a 2.7-fold increase in plaque area (Fig. 1C).

Although we cannot completely rule out an effect of formate on Henle-407 cells, experiments to find such an effect have been negative. Examination of the monolayers by light microscopy revealed no changes in morphology or cell density when Henle-407 cells were grown with 20 mM formate, and there was no effect on medium pH. Additionally, formate had no cytotoxic effects on Henle-407 cells, as measured by

lactate dehydrogenase release (Fig. S3A), and formate did not alter the growth of Henle-407 cells (Fig. S3B).

Listeria monocytogenes is another pathogen that, similarly to *Shigella*, accesses the host cell cytosol and exploits host actin polymerization for cell-to-cell spread. We postulated that if formate was affecting host cell physiology to promote bacterial cell-to-cell spread, it would increase the plaque size of *L. monocytogenes*, as well as *Shigella*. However, supplementation with exogenous formate had no significant effect on the plaque size of *L. monocytogenes* in Henle-407 cell monolayers (Fig. S5), further supporting the hypothesis that enhanced spread of intracellular *S. flexneri* in the presence of formate is a response by the bacteria, rather than the host cell.

The role of formate in increasing *Shigella* plaque size could be due to faster growth of the bacteria or increased spread. There was no significant difference in *S. flexneri* intracellular doubling time between the presence and absence of exogenous formate (Fig. 1D). However, we observed an increase in *S. flexneri* cell-to-cell spread in the presence of exogenous formate (Fig. 1E), suggesting that formate promotes *S. flexneri* cell-to-cell spread, resulting in increased plaque size in Henle-407 monolayers.

S. flexneri has only one known formate transporter, FocA. FocA is a bidirectional formate transporter that directly interacts with PFL to export formate (27–29). FocA activity is dependent on pH, and when the pH is below 5.8, the function of FocA switches to a formate importer (28). *focA* is cotranscribed with *pflB* and expressed under aerobic or microaerobic conditions under the control of ArcA and the fumarate and nitrate reduction regulator FNR (30–32). We found that mutating *S. flexneri focA* reduced plaque size similarly to the Δ*pflB* mutant, likely due to reduced formate secretion. However, plaque size of the Δ*focA* strain increased with exogenous formate (Fig. S4), indicating that *S. flexneri* formate import via FocA is dispensable for formate promotion of plaque size and suggesting that formate is sensed by *S. flexneri* outside the bacterial cytoplasm or, less probably, that formate is imported through an unidentified transporter.

***pflB* is required for *S. flexneri* formate secretion.** While *S. flexneri* metabolism is understudied, metabolism and mixed acid fermentation of the closely related bacterium *E. coli* have been characterized in detail, and the predominant *E. coli* fermentation products *in vitro* are formate, acetate, ethanol, and lactate (33). In limited oxygen, *E. coli* metabolizes carbon using glycolysis, producing pyruvate for mixed acid fermentation. Pyruvate is converted to lactate via lactate dehydrogenase or to acetyl-CoA via pyruvate dehydrogenase (PDH) or PFL; of these two enzyme complexes which generate acetyl-CoA, only PFL produces formate as a by-product. Acetyl-CoA is then converted to acetate or ethanol, while formate is predominantly secreted through one of two bidirectional transporters, FocA or FocB (28, 34). Cytoplasmic formate can be oxidized by the formate hydrogenlyase complex (FHL), while periplasmic formate can be oxidized by one of two formate dehydrogenase complexes (FDH-N or FDH-O). The genomes of *E. coli* and *S. flexneri* are highly similar, allowing us to project *S. flexneri* mixed acid fermentation (summarized in Fig. 2A). Of note, the *S. flexneri* locus containing *focA* and the PFL genes (including *pflB*) is highly conserved among sequenced *Shigella* species (Fig. S6). However, there are other notable differences in metabolism genes between *E. coli* and *S. flexneri*; *S. flexneri* has 58 metabolism-related pseudogenes compared to *E. coli,* including the putative formate transporter *focB*, and *fdhF*, a gene essential for the activity of FHL (35). We simulated *S. flexneri* metabolism *in silico* using a published *S. flexneri* genome-scale metabolic model (36, 37), which integrates *S. flexneri* genome data and enzyme stoichiometry of metabolic reactions into a metabolic network; constraint-based analysis is then applied to emulate metabolism maximizing biomass production (38, 39). To mimic intracellular conditions, we simulated a low-oxygen environment where carbon availability limits total growth. Under these conditions, *S. flexneri* is predicted to produce formate, acetate, and ethanol *in silico* at a ratio of approximately 3:2:1 and no lactate (Fig. 2A). The model predicted that 29.7% of total carbon available is converted to formate under the simulated conditions. This estima-

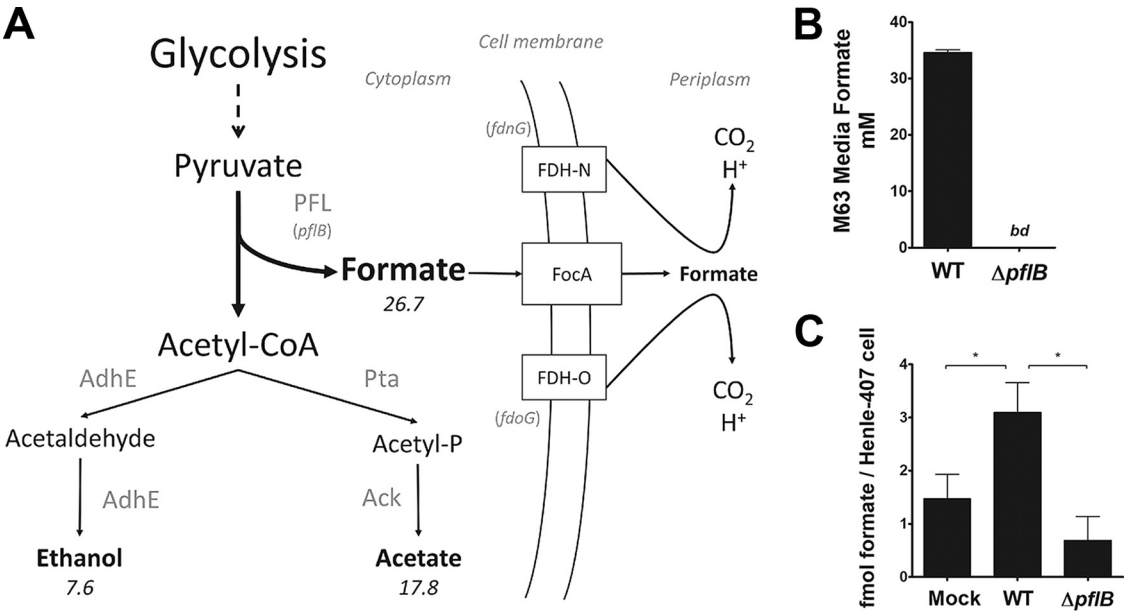

FIG 2 (A) Model of *S. flexneri* fermentative metabolism. *S. flexneri* metabolism was simulated using a genome-scale metabolic network model; numbers indicate relative carbon flux. Under anoxic conditions, *S. flexneri* is predicted to secrete formate, acetate, and ethanol at a ratio of approximately 3:2:1. Formate is a by-product of PFL-mediated conversion of pyruvate to acetyl-CoA. (B) *S. flexneri*-secreted formate was measured in the supernatant from bacteria grown anaerobically in M63 medium. *bd* indicates "below detection." No formate secretion was observed in the Δ*pflB* mutant. (C) Intracellular formate was measured in uninfected and infected Henle-407 cells at 3 hpi. Formate was normalized to the total number of Henle-407 cells. WT *S. flexneri* infection increased intracellular formate, while infection with the Δ*pflB* mutant did not.

tion is consistent with previous studies examining mixed acid fermentation in *S. flexneri* and *E. coli* (16, 40).

The amount of formate secreted by the *S. flexneri* WT and Δ*pflB* mutant was quantified from cells grown in minimal medium, under the conditions simulated in the *in silico* model. After 18 h of growth, the concentration of formate secreted by the WT *S. flexneri* strain was 34.6 ± 0.5 mM, translating to a 38.4% conversion of available carbon to formate (Fig. 2B). In contrast, there was no detectable formate in supernatants from the Δ*pflB* mutant, confirming that PFL is essential for *S. flexneri* formate production. At host cytosolic pH, formate exists as a monovalent anion that cannot passively diffuse across bacterial or eukaryotic cellular membranes, with the exception of acidic compartments such as lysosomes (21); we therefore postulated that host cytosolic formate concentration would increase during *S. flexneri* infection due to *S. flexneri* metabolism and the spatial restriction imposed by the host cell membrane. We observed a 2.1-fold increase in intracellular formate of infected cells compared to uninfected cells (Fig. 2C). In contrast, Henle-407 cells infected with the *S. flexneri* Δ*pflB* mutant showed no increase in intracellular formate concentration.

FDH-N inhibits *S. flexneri* plaque formation. *S. flexneri* encodes two periplasm-facing molybdoselenoformate dehydrogenase complexes, FDH-N and FDH-O, which couple formate oxidation to nitrate reduction. *E. coli* FDH-N, which catalyzes the conversion of periplasmic formate to H^+ and CO_2, is expressed during anaerobic growth and induced by nitrate in a NarL-dependent manner (41); FDH-O is active in the presence of oxygen and accounts for a smaller portion of the total formate dehydrogenase activity (42, 43). While *S. flexneri* PFL and FDH-N levels are elevated within an epithelial cell, expression of FDH-O-related genes is repressed (5, 15), suggesting that FDH-N is more important than FDH-O for formate metabolism by intracellular *S. flexneri*. If *S. flexneri* FDH-N is responsible for formate catabolism during intracellular growth, deletion of FDH-N would increase intracellular formate in infected Henle-407 cells and thus increase plaque size. We examined the plaque formation of *S. flexneri* Δ*fdnG* (catalytic subunit of FDH-N) and Δ*fdoG* (catalytic subunit of FDH-O) mutants. There was

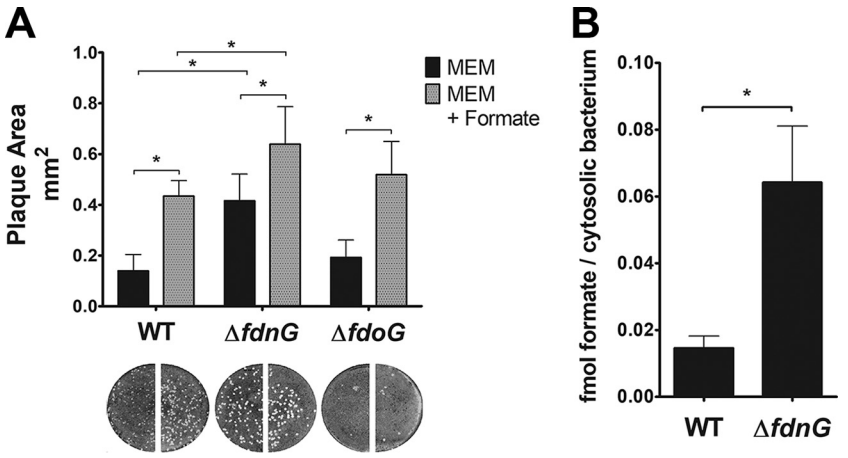

FIG 3 (A) The Δ*fdnG* mutant forms larger plaques. Plaque size of *S. flexneri* WT, FDH-N mutant (Δ*fdnG*), or FDH-O mutant (Δ*fdoG*) was measured; loss of FDH-N, which oxidizes formate to CO_2, increased plaque size. (B) Formate accumulates to higher levels in Henle-407 cells infected with the Δ*fdnG* mutant. Formate was normalized to the number of intracellular bacteria. An asterisk indicates statistical significance.

a 3.0-fold increase in plaque size of the *S. flexneri* Δ*fdnG* strain over WT (Fig. 3A). Furthermore, in the presence of exogenous formate the plaque size of the Δ*fdnG* strain increased 1.5-fold over the WT with formate. We measured formate levels of Henle-407 cells infected with *S. flexneri* WT and the Δ*fdnG* strain and found that formate was significantly higher in the Δ*fdnG* strain than the WT strain, consistent with reduced *S. flexneri* formate oxidation (Fig. 3B). These data indicate that FDH-N reduces *S. flexneri* spread, presumably by oxidizing formate derived from either *S. flexneri* or host metabolism and decreasing its concentration within the host cell cytosol. In contrast, the plaque size of the Δ*fdoG* strain was not significantly different from that of the WT strain, regardless of exogenous formate. This is consistent with the low expression of *fdoG* in intracellular bacteria (14). However, the Δ*fdoG* strain formed significantly fewer plaques than the WT strain, indicating that FDH-O, which is more highly expressed extracellularly, may be important for efficient invasion of host cells.

Formate alters *S. flexneri* virulence gene expression. To identify *S. flexneri* genes affected by formate that could promote plaque formation, we determined formate-induced differences in the *S. flexneri* transcriptome using RNA sequencing (RNA-seq). We were able to map an average of 3×10^6 unique reads per sample to the *S. flexneri* genome, and we found that exogenous formate significantly altered the expression of four genes on the virulence plasmid (Table 1). The *S. flexneri* gene *icsA*, which recruits host N-WASP for actin-mediated intercellular spread, was upregulated 2.1-fold by formate. Additionally, two *S. flexneri* T3SS effectors were upregulated approximately 2-fold by formate: *ipaJ* and *ipgD*. Formate also altered the expression of the virulence plasmid maintenance gene *ccdB* and 13 *S. flexneri* chromosomal genes (Table 1); however, we focused on *icsA*, *ipaJ*, and *ipgD*, since these genes are known virulence determinants.

To validate the findings of our RNA-seq, we quantified *S. flexneri icsA*, *ipaJ*, and *ipgD* transcript levels during growth *in vitro* or in Henle-407 cells using quantitative reverse transcriptase PCR (RT-qPCR). We observed significant sample-to-sample variation both *in vitro* and *in vivo*; however, formate supplementation significantly increased *S. flexneri icsA* and *ipaJ in vitro* (Fig. 4). We also observed that exogenous formate increased intracellular *S. flexneri ipaJ* expression 1.5-fold, while the Δ*pflB* mutant showed a 1.3-fold decrease in *ipaJ* expression compared to WT (Fig. 4). Both exogenous formate and *pflB* had no significant impact on *S. flexneri ipgD* levels either *in vitro* or in Henle-407 cells (Fig. 4).

Formate increases surface *S. flexneri* IcsA. *S. flexneri* uses polarly localized IcsA to recruit host N-WASP, catalyzing host actin synthesis and propelling the bacterium

TABLE 1 *S. flexneri* genes differentially regulated during infection of Henle-407 cells with exogenous 20 mM formate

Carriage location and gene	Function	Fold change
Virulence plasmid		
ipaJ	Host protein N-myristoylation	2.3
icsA/virG	Actin-mediated intercellular spread	2.1
ipgD	Host phosphoinositide metabolism	2.1
ccdB	Plasmid maintenance	−2.1
Chromosome		
yjhA	Hypothetical protein	3.3
yccJ	Hypothetical protein	2.5
yhaH	Putative cytochrome	2.3
rfbE	Polysaccharide biosynthesis	2.3
melR	Regulator of melibiose operon	2.1
ybeK	Putative tRNA synthetase	2.1
yjhT	Hypothetical protein	2.1
yhiO	Hypothetical protein	2.0
proV	Osmotic regulation	−2.1
Rnd	RNase D	−2.2
S2640	Hypothetical protein	−2.3
yebJ	Hypothetical protein	−2.4
ybaN	Hypothetical protein	−2.6

through the host cell cytosol (44, 45). Δ*icsA* mutants cannot spread and do not form plaques in Henle-407 monolayers (2, 46); therefore, to confirm that *S. flexneri icsA* is differentially regulated by formate, *S. flexneri* IcsA was visualized in infected Henle-407 cells by fluorescence staining and microscopy. IcsA labeled with fluorescein isothiocyanate (FITC) appeared as green, U-shaped foci on the micrographs that corresponded with the poles of intracellular bacteria, which were stained blue with 4′,6-diamidino-2-phenylindole (DAPI) (Fig. 5). As expected, no green foci were observed in cells infected with the Δ*icsA* mutant. We observed more *S. flexneri* with IcsA staining (45.8% ± 0.5%) in infected Henle-407 cells supplemented with formate than in those without formate supplementation (22.0% ± 6%), and the foci appeared brighter. In contrast, a smaller percentage of the intracellular *S. flexneri* Δ*pflB* mutant showed IcsA staining (7.0% ± 1.7%), and the foci were dimmer than with the WT strain. These findings together suggest that formate increases the levels of *S. flexneri* IcsA in infected Henle-407 cells.

***ipgD* is required for formate-mediated plaque formation.** *S. flexneri* IpgD is a secreted PtdIns(4,5)P_2 4-phosphatase that produces PtdIns5P in the host cell; increased PtdIns5P has widespread effects on the host, including alteration of host membrane

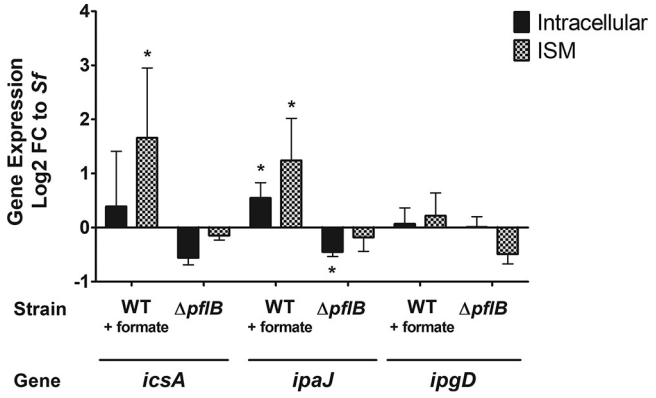

FIG 4 Formate increases the expression of *icsA* and *ipaJ*. *S. flexneri icsA*, *ipaJ*, and *ipgD* expression in Henle-407 cells at 3 hpi (black bars) or ISM (checkered bars) was independently determined by RT-qPCR. Log_2 fold change is relative to WT *S. flexneri*. An asterisk indicates statistical significance.

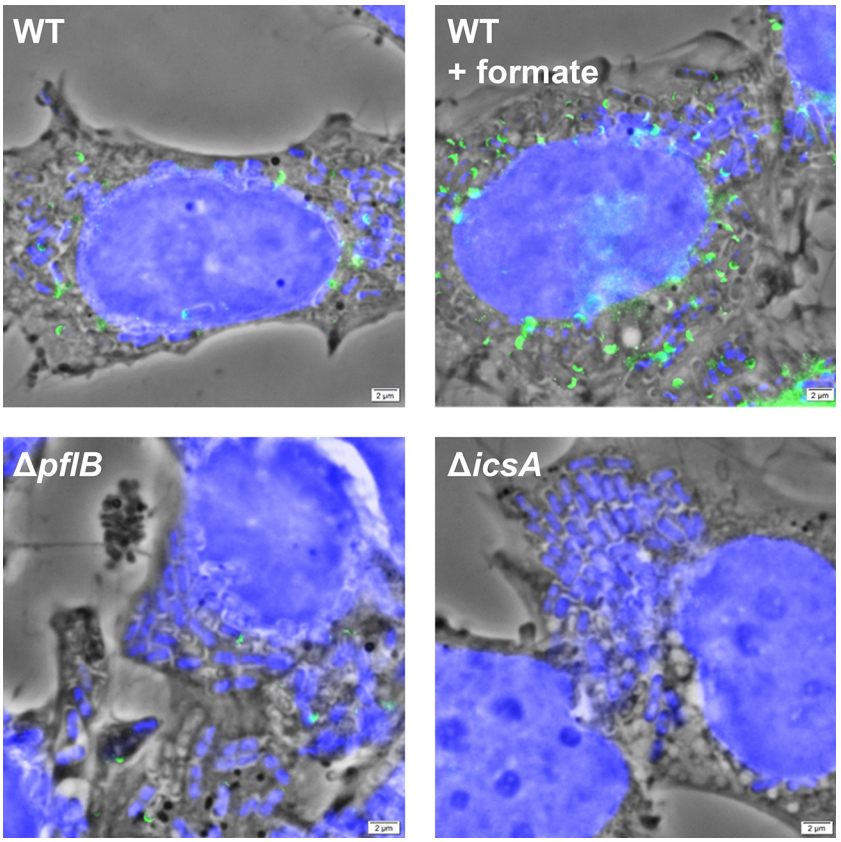

FIG 5 Formate increases *S. flexneri* IcsA in infected Henle-407 cells. Polarly localized IcsA (green) was visualized in intracellular *S. flexneri* (blue) using fluorescence microscopy. Fluorescence images were overlaid on a phase-contrast micrograph. We observed more polar IcsA WT *S. flexneri* grown with formate and lower polar IcsA levels in the Δ*pflB* mutant than in the WT strain.

tension, activation of host Akt kinase, inhibition of T-cell migration, inhibition of host extracellular ATP (eATP) secretion, activation of host ARF6, and altered host Ca^{2+} signaling (8, 47–50). To determine if *ipgD* is involved in the *S. flexneri* response to formate, we measured the plaque size of an *S. flexneri* Δ*ipgD* mutant in Henle-407 monolayers with exogenous formate. Compared to the *S. flexneri* WT strain, the Δ*ipgD* mutant formed smaller plaques (Fig. 6). Importantly, the Δ*ipgD* mutant showed no significant increase in plaque size when the tissue culture medium was supplemented with 20 mM formate. When *S. flexneri ipgD* was complemented on a plasmid, the formate-mediated increase in plaque size was restored (Fig. 6). This suggests that *ipgD* is required for the formate-mediated increase in *S. flexneri* plaque size.

***ipaJ* contributes to plaque size increase by formate.** IpaJ is an *S. flexneri*-secreted cysteine protease that disrupts the host Golgi apparatus by altering host protein N-myristoylation (11, 12, 51). We examined how the plaque size of an *S. flexneri* Δ*ipaJ* mutant changes in response to exogenous formate. We found that in the absence of exogenous formate, the mean plaque size of the Δ*ipaJ* mutant was not significantly different from that of the WT strain (Fig. 7), consistent with previous reports (52). The Δ*ipaJ* mutant response to formate was diminished compared to WT, with the mutant forming smaller plaques than the WT strain when both were supplemented with exogenous formate; this phenotype was complemented by providing *ipaJ* on a plasmid (Fig. 7). These results indicate that *ipaJ* contributes to the formate-mediated increase in *S. flexneri* plaque size.

***ipaJ* expression is dependent on *S. flexneri* cell density and formate.** Because *S. flexneri* secretes formate in the host cytosol as a by-product of carbon metabolism, and this formate accumulates in the host cytosol of *S. flexneri*-infected Henle-407 cells

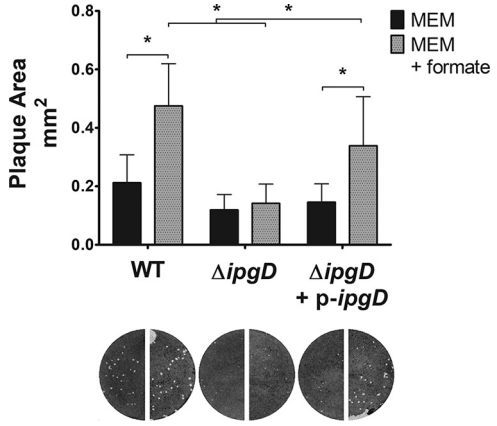

FIG 6 The *ipgD* mutant does not increase plaque size with formate. Plaque size of *S. flexneri* WT and Δ*ipgD* mutant was measured in cultured cells in the presence or absence of exogenous formate. (An asterisk indicates statistical significance.) The Δ*ipgD* mutant did not increase plaque size in the presence of exogenous formate, and this phenotype is complemented by providing *ipgD* on a plasmid.

(Fig. 2C), we expected that formate-induced virulence gene expression would increase as *S. flexneri* intracellular density increased, as formate is produced from bacterial metabolism. To test this, we constructed an *ipaJ* transcriptional reporter, in which the promoter region of *ipaJ* was fused to *gfp* on a plasmid, and *ipaJ* expression was visualized using fluorescence microscopy. We observed increased fluorescence in the intracellular *S. flexneri* WT cells compared to the Δ*pflB* mutant (Fig. 8A); likewise, formate supplementation of Henle-407 cells infected with WT *S. flexneri* increased fluorescence. Green fluorescent protein (GFP) fluorescence was then measured in single bacterial cells from fluorescence micrographs. We observed a 1.8-fold increase in *gfp* of *S. flexneri* when exogenous formate was added as a supplement (Fig. 8B), similar to the changes in *ipaJ* levels observed in previous experiments (Table 1 and Fig. 4). Likewise, we observed a 1.3-fold decrease of *ipaJ* expression in the Δ*pflB* mutant compared to the WT strain. We then measured the number of intracellular *S. flexneri* bacteria and the two-dimensional cell area of Henle-407 cells stained with wheat germ agglutinin (WGA) and regressed mean *ipaJ* expression of *S. flexneri* within individual Henle-407 cells on intracellular *S. flexneri* density. *ipaJ* expression positively correlated with *S. flexneri* intracellular density (Fig. 8C), and when cells were supplemented with exogenous formate, *ipaJ* expression levels were constitutively elevated regardless of intracellular *S.*

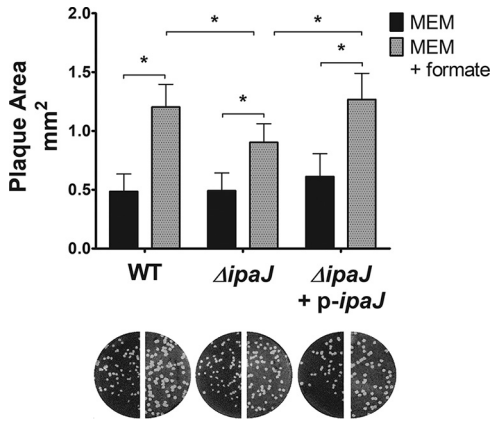

FIG 7 The *ipaJ* mutant has reduced response to formate. Plaque size of *S. flexneri* WT and Δ*ipaJ* mutant was measured in cultured cells in the presence or absence of exogenous formate. (An asterisk indicates statistical significance.) The difference in plaque size caused by the addition of exogenous formate is significantly less in the Δ*ipaJ* mutant than in the WT strain, and this phenotype is complemented by providing *ipaJ* on a plasmid.

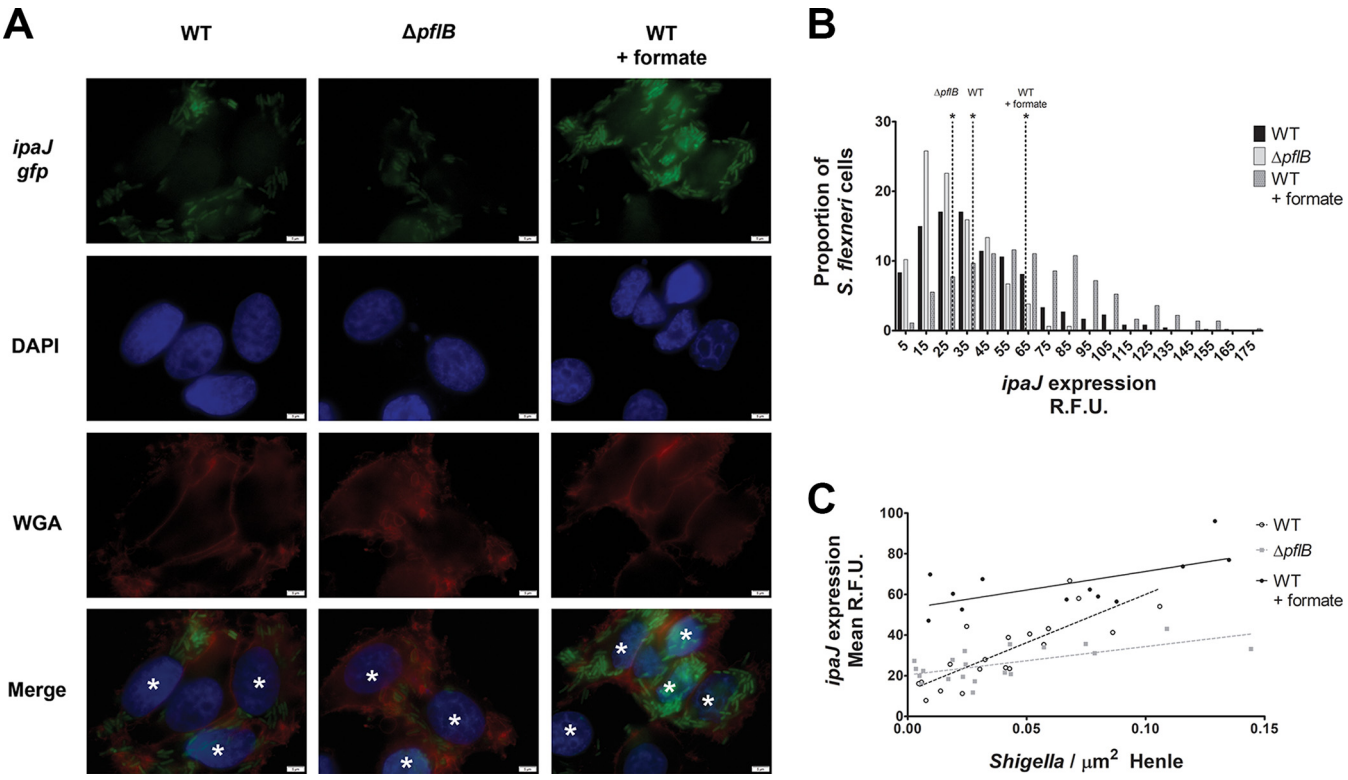

FIG 8 Expression of *ipaJ* in the intracellular environment increases in the presence of formate and is influenced by bacterial cell density and formate concentration in the Henle-407 cells. (A) The *ipaJ* promoter was fused to *gfp* (green), and infected Henle-407 cells were visualized using fluorescence microscopy. Nuclei were stained with DAPI (blue), and Henle-407 membranes were stained with wheat germ agglutinin (red). Asterisks indicate infected cells. The Δ*pflB* mutant displayed lower *gfp* intensity, while formate increased *gfp* intensity in WT. (B) *ipaJ* expression was measured by quantitative fluorescence microscopy. Dotted lines indicate median *gfp* intensity. An asterisk indicates statistical significance compared to each of the other two medians. Formate increased *ipaJ* expression 1.8-fold. (C) *ipaJ* expression of intracellular *S. flexneri* was regressed on *S. flexneri* density. The slope of WT *S. flexneri ipaJ* expression ($R^2 = 0.7$) was significantly different from that of WT plus formate ($R^2 = 0.4$) and the Δ*pflB* strain ($R^2 = 0.4$).

flexneri density. Furthermore, *ipaJ* expression of the Δ*pflB* mutant was lower than that of the WT strain, regardless of intracellular *S. flexneri* density. These data indicate that intracellular *ipaJ* expression is dependent on the intracellular density of *S. flexneri* cells, and this regulation is positively associated with formate accumulation.

Altering formate results in modified host response of *S. flexneri*-infected Henle-407 cells. *S. flexneri* infection elicits a strong inflammation response from the host cell (8, 53). To counteract this, *S. flexneri* employs IpaJ and IpgD, which dampen host interferon- and tumor necrosis factor (TNF)-stimulated genes (8, 11, 12). Because *ipgD* and *ipaJ* contribute to the *S. flexneri* response to formate (Fig. 6 and 7), we hypothesized that supplementation with exogenous formate would result in altered host immune response to *S. flexneri* infection. We selected 4 host genes known to be affected by either *ipgD* or *ipaJ*: CXCL10, interleukin-8 (IL-8), TNF-α, and TNFAIP3 (8, 11). We found that exogenous formate lowered the levels of CXCL10, IL-8, and TNFAIP3 in *S. flexneri*-infected Henle-407 cells (Fig. 9A, black bars), while in uninfected cells, exogenous formate had no effect on CXCL10, IL-8, TNF-α, or TNFAIP3 expression (1.0-, 1.1-, 0.9-, and 1.1-fold change, respectively).

Henle-407 cells, a HeLa derivative cell line, have altered immune pathways relating to *S. flexneri* infection response. For example, Henle-407 cells do not express the connexin hemichannels involved in secretion of eATP, a potent inflammatory signal (54). Therefore, we analyzed *S. flexneri*-infected CoN-841 cells grown with or without exogenous formate and quantified CXCL10, IL-8, TNF-α, or TNFAIP3 expression levels. We observed more gene expression variation in infected CoN-841 cells than in Henle-407 cells, and TNF-α was the most strongly repressed gene in infected CoN-841 cells supplemented with exogenous formate (Fig. 9A, checkered bars), suggesting that the

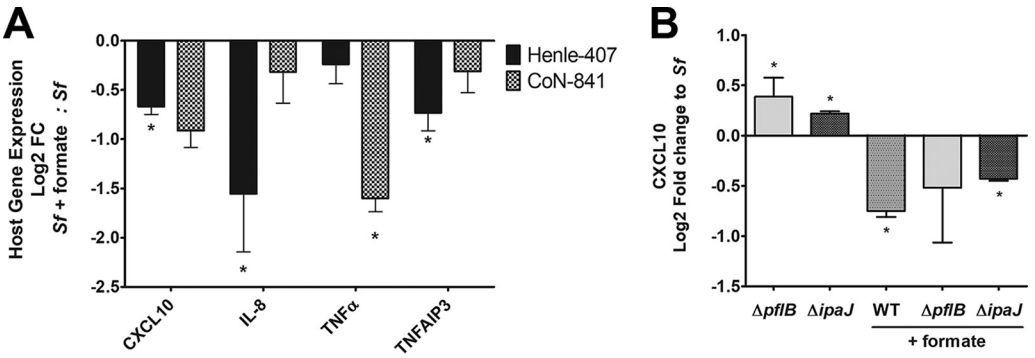

FIG 9 Formate inhibited interferon- and TNF-stimulated gene expression levels in infected Henle-407 and CoN-841 cells. (A) Host gene expression of infected Henle-407 cells (black bars) and CoN-841 cells (gray checkered bars) was determined by RT-qPCR. (B) CXCL10 transcript levels of Henle-407 cells infected with different *S. flexneri* strains were determined by RT-qPCR. Log_2 fold change is relative to host cells infected with WT *S. flexneri* in the absence of exogenous formate, and an asterisk indicates statistical significance compared to WT infection.

specific genes and the dynamics of the host immune response in regard to formate-regulated *S. flexneri* effectors vary in a different human cell line.

To confirm the effect of formate on *S. flexneri ipaJ*, we examined host CXCL10 expression in Henle-407 cells infected with the Δ*pflB* and Δ*ipaJ* mutant strains. In contrast to formate lowering CXCL10 expression in cells infected with WT *S. flexneri*, CXCL10 expression was increased in Henle-407 cells infected with the *S. flexneri* Δ*pflB* mutant, and this difference was abated when exogenous formate was provided as a supplement (Fig. 9B). Similarly to the Δ*pflB* mutant, CXCL10 expression was elevated in Henle-407 cells infected with the *S. flexneri* Δ*ipaJ* mutant, and formate reduced this response.

DISCUSSION

Formate is an important biomolecule for both human and bacterial metabolism. In bacteria, formate is a by-product of pyruvate formate lyase (PFL)-mediated conversion of pyruvate to acetyl-CoA. In addition to PFL, *Shigella* encodes a pyruvate dehydrogenase (PDH) complex that converts pyruvate to acetyl-CoA under aerobic conditions but does not produce formate. An *S. flexneri* Δ*aceE* mutant defective in PDH has an intracellular growth defect, indicating that PDH is utilized for acetyl-CoA generation within the host cell (16). Eukaryotic cells contain low levels of cytosolic oxygen, a condition that permits the activity of both PFL and PDH, which explains why the *S. flexneri* Δ*pflB* mutant intracellular growth rate is unaffected despite missing this source of acetyl-CoA (16).

Eukaryotic cells metabolize formate via one-carbon metabolism for purine biosynthesis, among other things (55). At biological pH, formate cannot passively cross bacterial or eukaryotic cell membranes (21); however, extracellular formate exchange occurs in cultured human cells (56–58), presumably facilitated through the formate transporter SLC26A6 (56, 59, 60). Likewise, formate is shuttled between the mitochondria and eukaryotic cytosol through an unknown mechanism (55). It is unclear how Henle-407 cells react to the influx of cytosolic formate from *S. flexneri* infection. We predict that a portion of *S. flexneri*-derived host cytosolic formate is oxidized by *S. flexneri* FDH-N (Fig. 3), a second portion is converted to purines by host one-carbon metabolism, and a third portion accumulates in the host cytosol.

Formate turnover has been previously linked to the intracellular growth phase of *S. flexneri* (5, 15). Here, we demonstrate that it is not the metabolism of formate but formate itself that promotes *S. flexneri* plaque formation by increasing intercellular spread via IcsA and modulating the host response to *S. flexneri* infection. While PFL can be reversed to convert formate to pyruvate for metabolism (61), formate increases Δ*pflB* mutant plaque size, indicating that formate is not used solely as a substrate for PFL to produce pyruvate for growth (Fig. 2B). And, while formate oxidation is a potential

source of NADH, we also show that formate oxidation is dispensable for intracellular *S. flexneri* metabolism, since exogenous formate does not increase *S. flexneri* growth rate within the host cell (Fig. 1C) and knocking out FDH-N promotes *S. flexneri* plaque formation (Fig. 4). Unlike the closely related *E. coli*, *Shigella* spp. (including *S. flexneri*) have a mutated FHL, suggesting an evolutionary selection against *Shigella* formate oxidation (35); however, formate dehydrogenases contribute to the fitness of closely related *E. coli* in the lumen during inflammation-associated colon dysbiosis (62), possibly explaining why *S. flexneri* maintains its formate dehydrogenases.

Although it is clear that extracellular formate can enter Henle-407 cells when provided as an exogenous supplement, as shown by uptake of radiolabeled formate (see Fig. S2 in the supplemental material) and alterations in *S. flexneri* gene expression (Table 1; Fig. 4 and 8), we believe that *Shigella*-derived formate is sufficient to differentially regulate expression related to intercellular spread and host immune dampening because we observe these phenotypes in *S. flexneri* formate metabolism mutants. We propose a model in which, following entry into the host cell cytoplasm, *S. flexneri* begins to replicate and metabolize host sugars and pyruvate, producing and secreting formate as a by-product. Formate accumulates in the infected cell cytosol rapidly due to the spatial constrictions of the host cell membrane and induces *icsA* to promote *S. flexneri* intercellular spread. Formate also induces the expression of *ipaJ* and possibly *ipgD* to alter the host immune response to *S. flexneri* infection. Because formate regulates *S. flexneri icsA* and *ipaJ* expression *in vitro* (Fig. 4), *S. flexneri* likely possesses a formate sensory mechanism; this *S. flexneri* formate sensor would likely act at the outer membrane or periplasm, as formate increases plaque size of the Δ*focA* formate transport mutant (Fig. S2). One possible sensing mechanism is the BarA-UvrY two-component regulatory system, which senses formate and short-chain fatty acids to modulate the activity of the Csr regulatory system in *E. coli* (63) and regulates virulence in *S. flexneri* and *Salmonella enterica* (25, 64). However, the fact that acetate fails to increase plaque size indicates that BarA-UvrY is not the sensory mechanism; consistent with this, we found that *S. flexneri* Δ*barA* or Δ*uvrY* mutants still increase plaque size in response to formate (Fig. S5).

Previous studies demonstrate that there is spatiotemporal regulation of *S. flexneri*-secreted effectors during host cell infection (5, 6, 65–67). Our data indicate that formate is an *S. flexneri* signal to differentially regulate *icsA* and *ipaJ* expression in the host cell, and this regulation is correlated with increased intracellular *S. flexneri* density. The dynamic nature of formate-mediated *S. flexneri* virulence gene regulation could explain the variation in both host and *S. flexneri* gene expression that we observed in response to formate (Fig. 4 and 9) and why there were inconsistencies such as formate-altered *S. flexneri ipgD* expression (Table 1 and Fig. 4). The production of formate is not essential to *S. flexneri* virulence, evidenced by the fact that the Δ*pflB* mutant is still able to form plaques, albeit smaller than those of the WT. Rather, formate-mediated regulation of *icsA/ipaJ* appears to be a way to fine-tune expression in response to intracellular bacterial density or to facilitate spread once a threshold density has been achieved. There is currently a high degree of interest in the complex relationship between metabolism and pathogenesis (68, 69), and the concept of a metabolic by-product regulating bacterial virulence is not new; one example is indole, a by-product of tryptophan hydrolysis that regulates virulence phenotypes and has been reported as a social signal in enteric microbial communities (70–72). It is easy to draw comparisons between indole and formate signaling; however, one notable difference between indole and formate signaling is that indole is diffusible across cellular membranes while formate is not (73), allowing cytosolic formate to accumulate during intracellular infection.

As the bacterial load within a host cell increases, so does the need of the bacteria to dampen the host immune response in order to evade host cytosolic defenses such as autophagy, as well as systemic defenses such as neutrophil recruitment and inflammation. Consistent with other pathogens that suppress host immune response, immunomodulating effectors secreted by a single *S. flexneri* cell, which are costly to produce,

benefit the entire intracellular *S. flexneri* population (74). Thus, we consider modulating host response to be a cooperative social behavior which conveys a benefit to *S. flexneri* intracellular populations. If formate sensing is social in nature, it could convey local information about both intracellular *S. flexneri* cell density and *S. flexneri* spatial constraint, as formate accumulation differs in the intracellular and extracellular environments. It should also be noted that inflammation in the colon results in higher levels of formate in the lumen (59). During *Shigella* infection, the *Shigella*-induced inflammatory response could lead to increased formate in the lumen and subsequently in the epithelial cells, promoting bacterial spread and production of anti-inflammatory effectors. A more complete understanding of the role of formate production and sensing in infected host cells will provide a better understanding of this complex host-pathogen interaction.

MATERIALS AND METHODS

Media and growth conditions. Bacterial strains, plasmids, and primers used in this study are listed in Table S1 in the supplemental material. *S. flexneri* was cultured on tryptic soy broth agar plates with 0.01% (wt/vol) Congo red (TSBA-CR), and red colonies were selected to ensure the presence of the *S. flexneri* virulence plasmid. Overnight bacterial cultures were grown in Luria-Bertani (LB) broth at 30°C, subcultured 1:100, and grown at 37°C to an optical density at 650 nm (OD_{650}) of 0.5 to 1.0 (mid-log phase) prior to infection. Deoxycholate (DOC) was added as a supplement at 0.1% (wt/vol) where indicated to increase efficiency of invasion of Henle-407 cultured cells (75). Antibiotics were added as supplements where indicated at the following concentrations: 25 μg/ml ampicillin, 50 μg/ml kanamycin, 6 μg/ml chloramphenicol, and 20 μg/ml gentamicin. Sodium formate was added as a supplement where indicated at 20 mM.

Henle-407 cells (ATCC intestinal 407, CCL-6) and CoN-841 cells (ATCC CCD 841, CRL-1790) were cultured in minimal essential medium (MEM; Gibco 61100-087) supplemented with 10% (vol/vol) Bacto tryptone phosphate broth (Difco), 10% (vol/vol) fetal bovine serum (Gibco 16140-071), 2 mM glutamine, and nonessential amino acids (Gibco 11140-050). Henle-407 and CoN-841 cells were grown at 37°C with 5% CO_2.

Construction of *S. flexneri* mutants and plasmids. Strains, primers, and plasmids used in this study are listed in Table S1. The Δ*fdnG*, Δ*fdoG,* and Δ*focA* mutants were created using P1 bacteriophage transduction of the genes from *E. coli* strains JW1470, JW3865, and JW0887 (respectively) from the Keio collection (76). The Δ*ipaJ* mutant was generated using a modified method of Datsenko and Wanner (77, 78). Overlap extension PCR was used to fuse 399 bp upstream and 383 bp downstream of *ipaJ* to each side of the chloramphenicol resistance cassette of pKD3 (77). This product was amplified by PCR using the ipaJKO-1 and ipaJKO-4 primers, ethanol precipitated, and brought to a concentration of >500 ng/μl in water. *S. flexneri* containing the plasmid pKD46 (77) was grown to mid-log phase in 25 ml LB with no NaCl at 30°C, and then 2 mM arabinose was added and the culture was brought to 37°C for 30 min. Cells were pelleted and resuspended in 500 μl warm water, mixed with 10 μl *ipaJ* knockout (KO) PCR product, and immediately electroporated. Mutants were selected on TSBA-CR with chloramphenicol. All mutants were verified by PCR and DNA sequencing at the University of Texas at Austin DNA sequencing facility.

The *ipaJ* complement plasmid (pBK24) was constructed by amplifying the *ipaJ* locus beginning ~400 bp upstream of the annotated *ipaJ* gene and ending at the *ipaJ* stop codon from *S. flexneri* DNA by PCR with primers ipaJ-30c-fw and ipaJ-30c-rv, containing 5′ KpnI and XbaI sites, respectively. After restriction digest, the product was ligated into the corresponding sites of the plasmid pWKS30 (79). The *ipaJ-gfp* transcriptional reporter plasmid (pBK25) was constructed by amplifying the *ipaJ* promoter region, beginning ~500 bp upstream of *ipaJ* and ending at the *ipaJ* start codon, by PCR using primers ipaJ-gfp-fw and ipaJ-gfp-rv containing 5′ SmaI and XbaI sites. After restriction digest, the product was ligated into the corresponding sites of the plasmid pLR29 (14). Both plasmids were confirmed by PCR and DNA sequencing at the University of Texas at Austin DNA sequencing facility.

***In silico* analysis of *S. flexneri* metabolism.** *In silico* metabolism simulations were performed using a previously published *S. flexneri* genome-scale metabolic network reconstruction (36) and OptFlux (37). We removed external boundary metabolites and used the core biomass production as our objective function and the pFBA simulation method. To simulate anaerobic growth in M63 medium, default environmental conditions were used, except that the lower bound of O_2 exchange was set to 0, the lower bound of nicotinate exchange was set to −0.162, and the lower bounds of glucose and pyruvate exchange were set to −10. Total biomass production was limited by carbon availability under these simulated conditions.

Tissue culture assays. Plaque assays were performed as described previously (18) with modifications (17). Bacteria at mid-log growth were centrifuged and resuspended in sterile saline to a final concentration of 5×10^4 CFU/ml, and 100 μl of this suspension was added to Henle-407 monolayers grown to confluence. Plates were centrifuged for 10 min at 1,000 × *g* and incubated for 60 min at 37°C and 5% CO_2. Monolayers were then washed four times with phosphate-buffered saline (PBS) and incubated in MEM supplemented with 0.2% glucose, gentamicin, and formate where indicated for either 48 or 72 h. Monolayers were stained with Wright-Giemsa stain (Camco) and imaged using an Alpha Innotech AlphaImager (Protein Simple), and plaque area was measured using ImageJ (80). Statistical significance

was determined by analysis of variance (ANOVA) with a Bonferroni posttest, $P < 0.05$ (GraphPad Prism); figures are representative of at least 2 independent experiments.

For *L. monocytogenes* plaque assays, *L. monocytogenes* was grown in brain heart infusion (BHI) broth for approximately 18 h at 30°C without shaking. One milliliter of culture was centrifuged at 13,000 × *g* for 2 min, and then the supernatant was removed and the pellet was resuspended in 1 ml PBS. Two microliters of *L. monocytogenes* suspension was added to Henle-407 monolayers grown in a 6-well plate and gently shaken for 1 min. The plate was incubated for 1 h at 37°C and 5% CO_2. The monolayers were then washed four times with PBS and incubated in MEM supplemented with 0.2% glucose, gentamicin (10 μg/ml), and formate where indicated for 48 to 72 h. Monolayers were stained with Wright-Giemsa stain (Camco) and imaged using an Alpha Innotech AlphaImager (Protein Simple), and plaque area was measured using ImageJ (80). Statistical significance was determined by Student's *t* test ($P < 0.05$; GraphPad Prism); figures are representative of 2 independent experiments.

To determine bacterial doubling time, Henle-407 monolayers in 6-well plates were infected as described for plaque assays with *S. flexneri* grown in deoxycholate and added at a multiplicity of infection (MOI) of 20. At 1 h postinfection (hpi) and every 30 min thereafter, one well was trypsinized and Henle-407 cells were then lysed in 1% deoxycholate, diluted, and spot plated on TSBA-CR. Doubling time (*r*) was determined using the formula $t \times \log_2/(\log y_2 - \log y_1)$, where *t* is time (150 min), y_1 is *Shigella* at 1 hpi, and y_2 is *Shigella* at 3.5 hpi ($n = 2$).

Cell-to-cell spread assays were performed as previously described (81). *S. flexneri* was added to Henle-407 cells at approximately 65% confluence at an MOI of 10. Cells were stained with Wright-Giemsa stain at 3 hpi, and cell-to-cell spread rates were calculated by counting approximately 100 infected Henle-407 cells adjacent to other Henle-407 cells. The proportion of *S. flexneri* spreading events was scored by determining if any Henle-407 cells adjacent to an infected cell also contained 3 or more internal bacterial cells. Statistical significance was determined by Student's *t* test ($n = 3$, $P < 0.05$).

Formate-induced cytotoxicity was determined by measuring secreted lactate dehydrogenase of Henle-407 cells supplemented with 20 mM formate every 24 h over 3 days using a lactate dehydrogenase assay (Sigma MAK066) according to the manufacturer's instructions. Statistical significance was determined using ANOVA with a Bonferroni posttest.

Formate uptake. The formate uptake assay was modified from a previous study (22). Briefly, Henle-407 cells were cultured in 30- by 10-mm plates, and 20 μM [^{14}C]formate (Moravek) was added to the tissue culture medium. Over the course of 48 h, cells were washed with PBS, trypsinized, and counted. Cells were then lysed directly in Optiphase HiSafe 3 (PerkinElmer). Counts per minute (cpm) was determined by scintillation, and counts were normalized to cell number and are relative to untreated cell lysates.

Formate quantification. For supernatant formate quantification, overnight cultures of *S. flexneri* WT and the indicated mutants were diluted 1:1,000 in M63 medium [100 mM KH_2PO_4, 15 mM $(NH_4)_2SO_4$, 1.8 μM $FeSO_4$, 1 mM $MgSO_4$, 162.5 nM nicotinic acid, 10 mM glucose, 10 mM pyruvate]. Cultures were grown for approximately 18 h at 37°C in sealed anaerobe jars containing anaerobic gas packs (BD 260651). The OD_{650} was recorded to determine bacterial growth. Cultures were then centrifuged, supernatants were filter sterilized prior to analysis using a formate assay (Sigma MAK059) according to the manufacturer's instructions, and samples were diluted 1:100 in formate assay buffer. Statistical significance was determined by ANOVA with a Bonferroni posttest ($P < 0.05$, $n = 3$) using GraphPad Prism.

For intracellular formate quantification, Henle-407 cells were infected with *S. flexneri* grown with deoxycholate as described above at an MOI of 5. At 5 hpi, Henle-407 monolayers were trypsinized and Henle-407 cells were counted using a Countess II cell counter (ThermoFisher). Where indicated, bacteria were quantified by plating. Cell pellets were then resuspended in 1 ml cold methanol-water (50:50) and incubated for 20 min on ice. Five hundred microliters of cold chloroform was added, and the mixture was vortexed and then centrifuged at 13,000 × *g* for 15 min. The aqueous phase was transferred to a new tube, liquid was evaporated using a vacuum manifold, and then samples were rehydrated in 100 μl formate assay buffer. Formate was quantified using the assay described above, and statistical significance was determined by either ANOVA with a Bonferroni posttest ($P < 0.05$, $n = 3$) or Student's *t* test ($P < 0.05$, $n = 3$). Results are representative of 2 independent experiments.

Phylogenetic analysis. For the phylogenetic analysis of the PFL locus, the PFL locus was identified in the 79 *Shigella* complete genomes currently represented in the NCBI database. The sequences were aligned using Geneious and had 96.2% identical sites. The PFL loci from other related gastrointestinal pathogens were included for comparison. A tree was built using the Geneious Tree Builder, using the Tamura-Nei model and neighbor joining method, with global alignment with free end gaps and a cost matrix at 51% similarity. The tree was visualized using FigTree (http://tree.bio.ed.ac.uk/software/figtree).

RNA extraction. For *in vitro* RNA extractions, *S. flexneri* was grown in intracellular salts medium (ISM) (4) supplemented with 10 mM pyruvate, RDM supplement (82), 20 mM bicarbonate, and 100 μM nitrate. Five-milliliter cultures were grown statically at 37°C with 5% CO_2 for 7 h. One milliliter of cold RNA-Stay (95% ethanol, 5% phenol) was added to each culture, and the entire volume was pelleted by centrifugation. One milliliter of cold RNA-Bee (Amsbio) was pipetted over the pellet. For RNA extractions of *S. flexneri*-infected Henle-407 cells, the Henle-407 cells were infected as described above with *S. flexneri* WT and mutants grown in deoxycholate and added at an MOI of 20. At 3 hpi, monolayers were washed once with PBS, and 1 ml of cold RNA-Bee (Amsbio) was pipetted over the monolayer. The cell lysates from either bacterial pellets or Henle-407 monolayers were transferred to new tubes, and 200 μl chloroform was added. The mixture was vortexed and after 5 min on ice was centrifuged at 13,000 × *g*, and the

upper aqueous phase was transferred to a new tube. RNA was then precipitated with isopropanol, treated with DNase I (Invitrogen), and solubilized in water.

cDNA library generation and RNA-seq. RNA from infected Henle-407 cells grown with and without formate and a mock uninfected sample was used to generate cDNA by the Genomic Sequencing and Analysis Facility (GSAF) at the University of Texas at Austin. Single samples from each condition tested were analyzed. RNA was checked for quality using a Bioanalyzer (Agilent); samples had an RNA integrity number (RIN) of >9. One microgram of total RNA was used for ribosome depletion using the Ribo-Zero Gold rRNA removal kit (Illumina) according to the manufacturer's instructions to eliminate both eukaryotic host rRNA and *Shigella* rRNA. The depleted RNA was fragmented to ~200 bp, and cDNA was generated using the NEBNext Ultra II directional RNA kit. Samples were barcoded, and single-end sequencing (75 cycles) of cDNA libraries was performed using a NextSeq 500 system (Illumina) at the GSAF. Sequencing generated 1.1×10^8 total reads for infected Henle-407 cells, and 1.0×10^8 total reads for infected Henle-407 cells grown with formate.

Read mapping and gene expression analysis. Sequence reads were aligned to the *S. flexneri* 2457T genome (GenBank accession no. AE014073.1) and the *S. flexneri* virulence plasmid pCP301 (GenBank accession no. AF386526.1) using CLC Genomics Workbench (Qiagen). Multimapped reads were excluded, as were genes containing reads that mapped to the *S. flexneri* genome or virulence plasmid in the mock treatment (listed in Table S2). Values of reads per kilobase per million (RPKM) were used for expression analysis, and genes with an RPKM value of <20 (arbitrary cutoff) were excluded. A Baggerley proportions test with a false-discovery rate correction was used to determine statistical significance ($P < 0.05$). Genes with a fold change greater than 2 were considered significantly different. A complete list of read mappings can be found in Table S2.

Quantitative reverse transcriptase PCR. RNA was quantified using a ND-1000 spectrophotometer (NanoDrop), and a total of 1 μg RNA was used with a high-capacity cDNA reverse transcription kit (Applied Biosystems). Two microliters of cDNA was then used as the template for SYBR green quantitative PCR (qPCR) (Applied Biosystems) using a ViiA 7 real-time PCR system (Applied Biosystems) at the University of Texas at Austin GSAF. Human gene expression was normalized to *actB*, and *Shigella* gene expression was normalized to *rssA*. All primers used for RT-qPCR are listed in Table S1. Statistical significance was determined using Student's *t* test of threshold cycle (ΔC_T) values compared to the *S. flexneri* WT-infected Henle-407 cells or *S. flexneri* WT grown in ISM.

Fluorescence microscopy. For IcsA labeling, Henle-407 cells were grown on glass coverslips in 6-well plates and infected with the *S. flexneri* WT, Δ*pflB*, or Δ*icsA* strain grown with deoxycholate (DOC) at an MOI of 1, as described above. At 3 hpi, cells were washed with PBS and then fixed with formaldehyde. Cells were then permeabilized with 0.5% Triton X-100, blocked with 5% bovine serum albumin (BSA) in PBS, and then incubated overnight with rabbit polyclonal antibody to IcsA (rabbit no. 5) provided by Edwin Oaks (Walter Reed Army Institute of Research) diluted 1:50 in PBS with 2.5% BSA. Cells were then washed with 0.05% Tween 20 in PBS and then blocked with 5% BSA in PBS for 30 min. The cells were then incubated with goat anti-rabbit IgG-FITC (sc-2012; Santa Cruz Biotechnology) diluted 1:1,000 and DAPI in PBS with 2.5% BSA for 2 h and then washed with 0.05% Tween 20 in PBS. Coverslips were then mounted on slides with Prolong Diamond antifade mountant (ThermoFisher). Images were then acquired using an Olympus BX41 microscope (100× objective) with a DP73 digital camera (Olympus) and processed using cellSens software (Olympus) or using a Zeiss LSM 710 confocal microscope (63× objective) at the University of Texas Microscopy and Imaging Facility. All exposures were identical, and images were processed in Photoshop (Adobe) to enhance contrast; all images were processed identically. Micrographs are representative of at least 3 independent experiments. To determine the proportion of intracellular bacteria with polar IcsA, the total number of bacteria and the number with polar IcsA staining were counted. Results shown are means ± standard deviations (SD) for the percent IcsA-positive bacteria in at least 4 fields.

S. flexneri strains containing the *ipaJ-gfp* reporter were grown with deoxycholate and ampicillin and diluted to an MOI of 1. Infections were carried out as described above, and at 3 hpi, cells were washed with PBS and formaldehyde fixed. Fixed cells were stained with wheat germ agglutinin (WGA)-Alexa Fluor 555 at 1 μg/ml. Slides were mounted with Vectashield with DAPI (Vector Laboratories), and images were acquired using an Olympus BX41 microscope (100× objective) with a DP73 digital camera (Olympus) and processed using cellSens software (Olympus). Acquisition of FITC (*gfp*) was fixed at 300 ms. Two-dimensional Henle-407 cell area was measured from the WGA membrane-labeled red channel, and *gfp* intensity of individual bacteria was quantified from the green channel using ImageJ (80). Background *gfp* fluorescence was measured in portions of each cell without bacteria and subtracted from individual bacterial cell fluorescence. A D'Agostino-Pearson normality test indicated that measurements did not conform to a Gaussian distribution. Therefore, statistical significance of *gfp* differences was determined by a Kruskal-Wallis test with a Dunn posttest ($P < 0.05$, $n > 300$). Regressions were performed using GraphPad Prism ($n = 12$ to 20), and slopes were found to be significantly different ($P < 0.05$).

Accession number. Sequencing data were deposited in GEO under accession number GSE119622.

SUPPLEMENTAL MATERIAL

Supplemental material for this article may be found at https://doi.org/10.1128/mBio.01777-18.

FIG S1, TIF file, 1.6 MB.

FIG S2, TIF file, 0.8 MB.

FIG S3, TIF file, 1.8 MB.

FIG S4, TIF file, 1.5 MB.
FIG S5, TIF file, 3.4 MB.
FIG S6, TIF file, 1.8 MB.
FIG S7, TIF file, 2.6 MB.
TABLE S1, DOCX file, 0.02 MB.
TABLE S2, XLSX file, 1.5 MB.

ACKNOWLEDGMENTS

We acknowledge A. R. Mey for reading and editing the manuscript and E. L. Bruger (ORCID: 0000-0002-6369-4180) and M. Shin for thoughtful discussions. We also thank C. F. Lesser for providing the Δ*ipgD* mutant, M. B. Goldberg for providing the *ipgD* complement plasmid, and E. V. Oaks and R. W. Kaminski for IcsA antiserum.

This work was funded by Public Health Service grant AI16935 from the National Institutes of Health to S.M.P.

REFERENCES

1. Wassef JS, Keren DF, Mailloux JL. 1989. Role of M cells in initial antigen uptake and in ulcer formation in the rabbit intestinal loop model of shigellosis. Infect Immun 57:858–863.
2. Bernardini ML, Mounier J, d'Hauteville H, Coquis-Rondon M, Sansonetti PJ. 1989. Identification of *icsA*, a plasmid locus of *Shigella flexneri* that governs bacterial intra- and intercellular spread through interaction with F-actin. Proc Natl Acad Sci U S A 86:3867–3871. https://doi.org/10.1073/pnas.86.10.3867.
3. Goldberg MB, Theriot JA. 1995. *Shigella flexneri* surface protein IcsA is sufficient to direct actin-based motility. Proc Natl Acad Sci U S A 92:6572–6576. https://doi.org/10.1073/pnas.92.14.6572.
4. Headley VL, Payne SM. 1990. Differential protein expression by *Shigella flexneri* in intracellular and extracellular environments. Proc Natl Acad Sci U S A 87:4179–4183. https://doi.org/10.1073/pnas.87.11.4179.
5. Lucchini S, Liu H, Jin Q, Hinton JCD, Yu J. 2005. Transcriptional adaptation of *Shigella flexneri* during infection of macrophages and epithelial cells: insights into the strategies of a cytosolic bacterial pathogen. Infect Immun 73:88–102. https://doi.org/10.1128/IAI.73.1.88-102.2005.
6. Campbell-Valois F-X, Schnupf P, Nigro G, Sachse M, Sansonetti PJ, Parsot C. 2014. A fluorescent reporter reveals on/off regulation of the *Shigella* type III secretion apparatus during entry and cell-to-cell spread. Cell Host Microbe 15:177–189. https://doi.org/10.1016/j.chom.2014.01.005.
7. Ashida H, Mimuro H, Sasakawa C. 2015. *Shigella* manipulates host immune responses by delivering effector proteins with specific roles. Front Immunol 6:219. https://doi.org/10.3389/fimmu.2015.00219.
8. Puhar A, Tronchere H, Payrastre B, Nhieu GT, Sansonetti PJ. 2013. A *Shigella* effector dampens inflammation by regulating epithelial release of danger signal ATP through production of the lipid mediator PtdIns5P. Immunity 39:1121–1131. https://doi.org/10.1016/j.immuni.2013.11.013.
9. Mounier J, Boncompain G, Senerovic L, Lagache T, Chretien F, Perez F, Kolbe M, Olivo-Marin JC, Sansonetti PJ, Sauvonnet N. 2012. *Shigella* effector IpaB-induced cholesterol relocation disrupts the Golgi complex and recycling network to inhibit host cell secretion. Cell Host Microbe 12:381–389. https://doi.org/10.1016/j.chom.2012.07.010.
10. Dong N, Zhu Y, Lu Q, Hu L, Zheng Y, Shao F. 2012. Structurally distinct bacterial TBC-like GAPs link Arf GTPase to Rab1 inactivation to counteract host defenses. Cell 150:1029–1041. https://doi.org/10.1016/j.cell.2012.06.050.
11. Burnaevskiy N, Fox TG, Plymire DA, Ertelt JM, Weigele BA, Selyunin AS, Way SS, Patrie SM, Alto NM. 2013. Proteolytic elimination of N-myristoyl modifications by the *Shigella* virulence factor IpaJ. Nature 496:106–109. https://doi.org/10.1038/nature12004.
12. Dobbs N, Burnaevskiy N, Chen D, Gonugunta VK, Alto NM, Yan N. 2015. STING activation by translocation from the ER is associated with infection and autoinflammatory disease. Cell Host Microbe 18:157–168. https://doi.org/10.1016/j.chom.2015.07.001.
13. Zheng Z, Wei C, Guan K, Yuan Y, Zhang Y, Ma S, Cao Y, Wang F, Zhong H, He X. 2016. Bacterial E3 ubiquitin ligase IpaH4.5 of *Shigella flexneri* targets TBK1 to dampen the host antibacterial response. J Immunol 196:1199–1208. https://doi.org/10.4049/jimmunol.1501045.
14. Runyen-Janecky LJ, Payne SM. 2002. Identification of chromosomal *Shigella flexneri* genes induced by the eukaryotic intracellular environment. Infect Immun 70:4379–4388. https://doi.org/10.1128/IAI.70.8.4379-4388.2002.
15. Pieper R, Fisher CR, Suh M-J, Huang S-T, Parmar P, Payne SM. 2013. Analysis of the proteome of intracellular *Shigella flexneri* reveals pathways important for intracellular growth. Infect Immun 81:4635–4648. https://doi.org/10.1128/IAI.00975-13.
16. Kentner D, Martano G, Callon M, Chiquet P, Brodmann M, Burton O, Wahlander A, Nanni P, Delmotte N, Grossmann J, Limenitakis J, Schlapbach R, Kiefer P, Vorholt JA, Hiller S, Bumann D. 2014. *Shigella* reroutes host cell central metabolism to obtain high-flux nutrient supply for vigorous intracellular growth. Proc Natl Acad Sci U S A 111:9929–9934. https://doi.org/10.1073/pnas.1406694111.
17. Waligora EA, Fisher CR, Hanovice NJ, Rodou A, Wyckoff EE, Payne SM. 2014. Role of intracellular carbon metabolism pathways in *Shigella flexneri* virulence. Infect Immun 82:2746–2755. https://doi.org/10.1128/IAI.01575-13.
18. Oaks EV, Wingfield ME, Formal SB. 1985. Plaque formation by virulent *Shigella flexneri*. Infect Immun 48:124–129.
19. Fisher CR, Davies NM, Wyckoff EE, Feng Z, Oaks EV, Payne SM. 2009. Genetics and virulence association of the *Shigella flexneri* sit iron transport system. Infect Immun 77:1992–1999. https://doi.org/10.1128/IAI.00064-09.
20. Cersini A, Salvia AM, Bernardini ML. 1998. Intracellular multiplication and virulence of *Shigella flexneri* auxotrophic mutants. Infect Immun 66:549–557.
21. Saleh AM, Rudnick H, Aronson PS. 1996. Mechanism of H^+-coupled formate transport in rabbit renal microvillus membranes. Am J Physiol 271:F401–F407. https://doi.org/10.1152/ajprenal.1996.271.2.F401.
22. Patel H, Pietro ED, MacKenzie RE. 2003. Mammalian fibroblasts lacking mitochondrial NAD^+-dependent methylenetetrahydrofolate dehydrogenase-cyclohydrolase are glycine auxotrophs. J Biol Chem 278:19436–19441. https://doi.org/10.1074/jbc.M301718200.
23. Laerke HN, Jensen BB. 1999. D-tagatose has low small intestinal digestibility but high large intestinal fermentability in pigs. J Nutr 129:1002–1009. https://doi.org/10.1093/jn/129.5.1002.
24. Laerke HN, Jensen BB, Højsgaard S. 2000. In vitro fermentation pattern of D-tagatose is affected by adaptation of the microbiota from the gastrointestinal tract of pigs. J Nutr 130:1772–1779. https://doi.org/10.1093/jn/130.7.1772.
25. Huang Y, Suyemoto M, Garner CD, Cicconi KM, Altier C. 2008. Formate acts as a diffusible signal to induce *Salmonella* invasion. J Bacteriol 190:4233–4241. https://doi.org/10.1128/JB.00205-08.
26. Zoetendal EG, Raes J, van den Bogert B, Arumugam M, Booijink CC, Troost FJ, Bork P, Wels M, de Vos WM, Kleerebezem M. 2012. The human small intestinal microbiota is driven by rapid uptake and conversion of simple carbohydrates. ISME J 6:1415–1426. https://doi.org/10.1038/ismej.2011.212.
27. Wang Y, Huang Y, Wang J, Cheng C, Huang W, Lu P, Xu YN, Wang P, Yan N, Shi Y. 2009. Structure of the formate transporter FocA reveals a pentameric aquaporin-like channel. Nature 462:467–472. https://doi.org/10.1038/nature08610.
28. Lu W, Du J, Schwarzer NJ, Gerbig-Smentek E, Einsle O, Andrade SL. 2012.

The formate channel FocA exports the products of mixed-acid fermentation. Proc Natl Acad Sci U S A 109:13254–13259. https://doi.org/10.1073/pnas.1204201109.

29. Doberenz C, Zorn M, Falke D, Nannemann D, Hunger D, Beyer L, Ihling CH, Meiler J, Sinz A, Sawers RG. 2014. Pyruvate formate-lyase interacts directly with the formate channel FocA to regulate formate translocation. J Mol Biol 426:2827–2839. https://doi.org/10.1016/j.jmb.2014.05.023.
30. Sawers G, Suppmann B. 1992. Anaerobic induction of pyruvate formate-lyase gene expression is mediated by the ArcA and FNR proteins. J Bacteriol 174:3474–3478. https://doi.org/10.1128/jb.174.11.3474-3478.1992.
31. Sawers G. 1993. Specific transcriptional requirements for positive regulation of the anaerobically inducible *pfl* operon by ArcA and FNR. Mol Microbiol 10:737–747. https://doi.org/10.1111/j.1365-2958.1993.tb00944.x.
32. Partridge JD, Sanguinetti G, Dibden DP, Roberts RE, Poole RK, Green J. 2007. Transition of *Escherichia coli* from aerobic to micro-aerobic conditions involves fast and slow reacting regulatory components. J Biol Chem 282:11230–11237. https://doi.org/10.1074/jbc.M700728200.
33. Clark DP. 1989. The fermentation pathways of *Escherichia coli*. FEMS Microbiol Rev 5:223–234.
34. Beyer L, Doberenz C, Falke D, Hunger D, Suppmann B, Sawers RG. 2013. Coordination of FocA and pyruvate formate-lyase synthesis in *Escherichia coli* demonstrates preferential translocation of formate over other mixed-acid fermentation products. J Bacteriol 195:1428–1435. https://doi.org/10.1128/JB.02166-12.
35. Wei J, Goldberg MB, Burland V, Venkatesan MM, Deng W, Fournier G, Mayhew GF, Plunkett G, Rose DJ, Darling A, Mau B, Perna NT, Payne SM, Runyen-Janecky LJ, Zhou S, Schwartz DC, Blattner FR. 2003. Complete genome sequence and comparative genomics of *Shigella flexneri* serotype 2a strain 2457T. Infect Immun 71:2775–2786. https://doi.org/10.1128/IAI.71.5.2775-2786.2003.
36. Monk JM, Charusanti P, Aziz RK, Lerman JA, Premyodhin N, Orth JD, Feist AM, Palsson BO. 2013. Genome-scale metabolic reconstructions of multiple *Escherichia coli* strains highlight strain-specific adaptations to nutritional environments. Proc Natl Acad Sci U S A 110:20338–20343. https://doi.org/10.1073/pnas.1307797110.
37. Rocha I, Maia P, Evangelista P, Vilaca P, Soares S, Pinto JP, Nielsen J, Patil KR, Ferreira EC, Rocha M. 2010. OptFlux: an open-source software platform for in silico metabolic engineering. BMC Syst Biol 4:45. https://doi.org/10.1186/1752-0509-4-45.
38. Oberhardt MA, Palsson BO, Papin JA. 2009. Applications of genome-scale metabolic reconstructions. Mol Syst Biol 5:320. https://doi.org/10.1038/msb.2009.77.
39. Feist AM, Herrgard MJ, Thiele I, Reed JL, Palsson BO. 2009. Reconstruction of biochemical networks in microorganisms. Nat Rev Microbiol 7:129–143. https://doi.org/10.1038/nrmicro1949.
40. Zhu J, Shimizu K. 2004. The effect of *pfl* gene knockout on the metabolism for optically pure D-lactate production by *Escherichia coli*. Appl Microbiol Biotechnol 64:367–375. https://doi.org/10.1007/s00253-003-1499-9.
41. Wang H, Gunsalus RP. 2003. Coordinate regulation of the *Escherichia coli* formate dehydrogenase *fdnGHI* and *fdhF* genes in response to nitrate, nitrite, and formate: roles for NarL and NarP. J Bacteriol 185:5076–5085. https://doi.org/10.1128/JB.185.17.5076-5085.2003.
42. Darwin A, Tormay P, Page L, Griffiths L, Cole J. 1993. Identification of the formate dehydrogenases and genetic determinants of formate-dependent nitrite reduction by *Escherichia coli* K12. J Gen Microbiol 139:1829–1840. https://doi.org/10.1099/00221287-139-8-1829.
43. Abaibou H, Pommier J, Benoit S, Giordano G, Mandrand-Berthelot MA. 1995. Expression and characterization of the *Escherichia coli fdo* locus and a possible physiological role for aerobic formate dehydrogenase. J Bacteriol 177:7141–7149. https://doi.org/10.1128/jb.177.24.7141-7149.1995.
44. Goldberg MB. 2001. Actin-based motility of intracellular microbial pathogens. Microbiol Mol Biol Rev 65:595–626. https://doi.org/10.1128/MMBR.65.4.595-626.2001.
45. Suzuki T, Sasakawa C. 2001. Molecular basis of the intracellular spreading of *Shigella*. Infect Immun 69:5959–5966. https://doi.org/10.1128/IAI.69.10.5959-5966.2001.
46. Rossi RM, Yum L, Agaisse H, Payne SM. 2017. Cardiolipin synthesis and outer membrane localization are required for *Shigella flexneri* virulence. mBio 8:e01199-17. https://doi.org/10.1128/mBio.01199-17.
47. Niebuhr K, Giuriato S, Pedron T, Philpott DJ, Gaits F, Sable J, Sheetz MP, Parsot C, Sansonetti PJ, Payrastre B. 2002. Conversion of PtdIns(4,5)P_2 into PtdIns(5)P by the *S. flexneri* effector IpgD reorganizes host cell morphology. EMBO J 21:5069–5078. https://doi.org/10.1093/emboj/cdf522.
48. Pendaries C, Tronchere H, Arbibe L, Mounier J, Gozani O, Cantley L, Fry MJ, Gaits-Iacovoni F, Sansonetti PJ, Payrastre B. 2006. PtdIns5P activates the host cell PI3-kinase/Akt pathway during *Shigella flexneri* infection. EMBO J 25:1024–1034. https://doi.org/10.1038/sj.emboj.7601001.
49. Garza-Mayers AC, Miller KA, Russo BC, Nagda DV, Goldberg MB. 2015. *Shigella flexneri* regulation of ARF6 activation during bacterial entry via an IpgD-mediated positive feedback loop. mBio 6:e02584-14. https://doi.org/10.1128/mBio.02584-14.
50. Sun CH, Wacquier B, Aguilar DI, Carayol N, Denis K, Boucherie S, Valencia-Gallardo C, Simsek C, Erneux C, Lehman A, Enninga J, Arbibe L, Sansonetti P, Dupont G, Combettes L, Tran Van Nhieu G. 2017. The *Shigella* type III effector IpgD recodes Ca^{2+} signals during invasion of epithelial cells. EMBO J 36:2567–2580. https://doi.org/10.15252/embj.201696272.
51. Slagowski NL, Kramer RW, Morrison MF, LaBaer J, Lesser CF. 2008. A functional genomic yeast screen to identify pathogenic bacterial proteins. PLoS Pathog 4:e9. https://doi.org/10.1371/journal.ppat.0040009.
52. Buysse JM, Dunyak DS, Hartman AB, Venkatesan MM. 1997. Identification and molecular characterization of a 27 kDa *Shigella flexneri* invasion plasmid antigen, IpaJ. Microb Pathog 23:357–369. https://doi.org/10.1006/mpat.1997.0164.
53. Perry AK, Chen G, Zheng D, Tang H, Cheng G. 2005. The host type I interferon response to viral and bacterial infections. Cell Res 15:407–422. https://doi.org/10.1038/sj.cr.7290309.
54. Elfgang C, Eckert R, Lichtenberg-Fraté H, Butterweck A, Traub O, Klein RA, Hülser DF, Willecke K. 1995. Specific permeability and selective formation of gap junction channels in connexin-transfected HeLa cells. J Cell Physiol 129:805–817.
55. Brosnan ME, Brosnan JT. 2016. Formate: the neglected member of one-carbon metabolism. Annu Rev Nutr 36:369–388. https://doi.org/10.1146/annurev-nutr-071715-050738.
56. Aronson PS. 2006. Essential roles of CFEX-mediated Cl-oxalate exchange in proximal tubule NaCl transport and prevention of urolithiasis. Kidney Int 70:1207–1213. https://doi.org/10.1038/sj.ki.5001741.
57. Meiser J, Vazquez A. 2016. Give it or take it: the flux of one-carbon in cancer cells. FEBS J 283:3695–3704. https://doi.org/10.1111/febs.13731.
58. Bao XR, Ong SE, Goldberger O, Peng J, Sharma R, Thompson DA, Vafai SB, Cox AG, Marutani E, Ichinose F, Goessling W, Regev A, Carr SA, Clish CB, Mootha VK. 2016. Mitochondrial dysfunction remodels one-carbon metabolism in human cells. Elife 5:e10575. https://doi.org/10.7554/eLife.10575.
59. Wang Z, Petrovic S, Mann E, Soleimani M. 2002. Identification of an apical Cl^-/HCO_3^- exchanger in the small intestine. Am J Physiol Gastrointest Liver Physiol 282:G573–G579. https://doi.org/10.1152/ajpgi.00338.2001.
60. Nozawa T, Sugiura S, Hashino Y, Tsuji A, Tamai I. 2004. Role of anion exchange transporter PAT1 (SLC26A6) in intestinal absorption of organic anions. J Drug Target 12:97–104. https://doi.org/10.1080/10611860410001693742.
61. Zelcbuch L, Lindner SN, Zegman Y, Vainberg Slutskin I, Antonovsky N, Gleizer S, Milo R, Bar-Even A. 2016. Pyruvate formate-lyase enables efficient growth of *Escherichia coli* on acetate and formate. Biochemistry 55:2423–2426. https://doi.org/10.1021/acs.biochem.6b00184.
62. Hughes ER, Winter MG, Duerkop BA, Spiga L, Furtado de Carvalho T, Zhu W, Gillis CC, Büttner L, Smoot MP, Behrendt CL, Cherry S, Santos RL, Hooper LV, Winter SE. 2017. Microbial respiration and formate oxidation as metabolic signatures of inflammation-associated dysbiosis. Cell Host Microbe 21:208–219. https://doi.org/10.1016/j.chom.2017.01.005.
63. Chavez RG, Alvarez AF, Romeo T, Georgellis D. 2010. The physiological stimulus for the BarA sensor kinase. J Bacteriol 192:2009–2012. https://doi.org/10.1128/JB.01685-09.
64. Gore AL, Payne SM. 2010. CsrA and Cra influence *Shigella flexneri* pathogenesis. Infect Immun 78:4674–4682. https://doi.org/10.1128/IAI.00589-10.
65. Demers B, Sansonetti PJ, Parsot C. 1998. Induction of type III secretion in *Shigella flexneri* is associated with differential control of transcription of genes encoding secreted proteins. EMBO J 17:2894–2903. https://doi.org/10.1093/emboj/17.10.2894.
66. Enninga J, Mounier J, Sansonetti P, Tran Van Nhieu G. 2005. Secretion of type III effectors into host cells in real time. Nat Methods 2:959–965. https://doi.org/10.1038/nmeth804.
67. Ehsani S, Santos JC, Rodrigues CD, Henriques R, Audry L, Zimmer C, Sansonetti P, Tran Van Nhieu G, Enninga J. 2012. Hierarchies of host factor

dynamics at the entry site of *Shigella* flexneri during host cell invasion. Infect Immun 80:2548–2557. https://doi.org/10.1128/IAI.06391-11.
68. Rohmer L, Hocquet D, Miller SI. 2011. Are pathogenic bacteria just looking for food? Metabolism and microbial pathogenesis. Trends Microbiol 19:341–348. https://doi.org/10.1016/j.tim.2011.04.003.
69. Olive AJ, Sassetti CM. 2016. Metabolic crosstalk between host and pathogen: sensing, adapting and competing. Nat Rev Microbiol 14:221–234. https://doi.org/10.1038/nrmicro.2016.12.
70. Ahmer BM. 2004. Cell-to-cell signalling in *Escherichia coli* and *Salmonella enterica*. Mol Microbiol 52:933–945. https://doi.org/10.1111/j.1365-2958.2004.04054.x.
71. Lee JH, Lee J. 2010. Indole as an intercellular signal in microbial communities. FEMS Microbiol Rev 34:426–444. https://doi.org/10.1111/j.1574-6976.2009.00204.x.
72. Kim J, Park W. 2015. Indole: a signaling molecule or a mere metabolic byproduct that alters bacterial physiology at a high concentration? J Microbiol 53:421–428. https://doi.org/10.1007/s12275-015-5273-3.
73. Pinero-Fernandez S, Chimerel C, Keyser UF, Summers DK. 2011. Indole transport across *Escherichia coli* membranes. J Bacteriol 193:1793–1798. https://doi.org/10.1128/JB.01477-10.
74. Rundell EA, McKeithen-Mead SA, Kazmierczak BI. 2016. Rampant cheating by pathogens? PLoS Pathog 12:e1005792. https://doi.org/10.1371/journal.ppat.1005792.
75. Pope LM, Reed KE, Payne SM. 1995. Increased protein secretion and adherence to HeLa cells by *Shigella* spp. following growth in the presence of bile salts. Infect Immun 63:3642–3648.
76. Baba T, Ara T, Hasegawa M, Takai Y, Okumura Y, Baba M, Datsenko KA, Tomita M, Wanner BL, Mori H. 2006. Construction of *Escherichia coli* K-12 in-frame, single-gene knockout mutants: the Keio collection. Mol Syst Biol 2:2006.0008. https://doi.org/10.1038/msb4100050.
77. Datsenko KA, Wanner BL. 2000. One-step inactivation of chromosomal genes in *Escherichia coli* K-12 using PCR products. Proc Natl Acad Sci U S A 97:6640–6645. https://doi.org/10.1073/pnas.120163297.
78. Zurawski DV, Mitsuhata C, Mumy KL, McCormick BA, Maurelli AT. 2006. OspF and OspC1 are *Shigella flexneri* type III secretion system effectors that are required for postinvasion aspects of virulence. Infect Immun 74:5964–5976. https://doi.org/10.1128/IAI.00594-06.
79. Wang RF, Kushner SR. 1991. Construction of versatile low-copy-number vectors for cloning, sequencing and gene expression in *Escherichia coli*. Gene 100:195–199. https://doi.org/10.1016/0378-1119(91)90366-J.
80. Rasband WS. 1997. ImageJ. US National Institutes of Health, Bethesda, MD. http://imagej.nih.gov/ij/.
81. Carpenter CD, Cooley BJ, Needham BD, Fisher CR, Trent MS, Gordon V, Payne SM. 2014. The Vps/VacJ ABC transporter is required for intercellular spread of *Shigella flexneri*. Infect Immun 82:660–669. https://doi.org/10.1128/IAI.01057-13.
82. Sharma AK, Payne SM. 2006. Induction of expression of *hfq* by DksA is essential for *Shigella flexneri* virulence. Mol Microbiol 62:469–479. https://doi.org/10.1111/j.1365-2958.2006.05376.x.